Chapter 4

Fast Multidimensional NMR by Hadamard Spectroscopy

Ray Freeman[1] and Ēriks Kupče[2]

[1]*Jesus College, Cambridge University, Cambridge, CB5 8BP, UK*
[2]*Varian Ltd, 6 Mead Road, Yarnton, Oxford, OX5 1QU, UK*

4.1 INTRODUCTION

Many of us may have used a Hadamard matrix without realizing it. It often happens that a physical measurement results in two quantities $A + B$ and $A - B$, where in fact the desired parameters are A and B. In NMR, for example, coupling constants can be measured in crowded spectra using the "in-phase antiphase" method.[1] We solve this trivial problem by taking the sum ($2A$) and the difference ($2B$), implicitly utilizing the simplest Hadamard matrix $\boldsymbol{H}_2$, which can be written in three equivalent ways:

$$\begin{array}{cccccc} + & + & +1 & +1 & 1 & 1 \\ + & - & +1 & -1 & 1 & 0 \end{array} \qquad (4.1)$$

or indeed represented as two differently colored "tiles" following the same pattern. The phase cycles of many NMR sequences implicitly invoke higher-order Hadamard matrices; for example, the heteronuclear multiple quantum correlation (HMQC) experiment[2] cycles the radiofrequency pulse phases ϕ_1, ϕ_2, ϕ_3 and the receiver phase ϕ_4 according to the Hadamard matrix of order four:

$$\begin{array}{l} \phi_1 \; + + + + \\ \phi_2 \; + - + - \\ \phi_3 \; + + - - \\ \phi_4 \; + - - + \end{array} \qquad (4.2)$$

Hadamard matrices were first proposed by Sylvester in 1867, some 26 years before they were considered by Hadamard[3] himself. A Hadamard matrix $\boldsymbol{H}_N$ of order N is a square matrix whose rows are mutually orthogonal. There are Hadamard matrices for all orders 2^k where k is a positive integer. If $\boldsymbol{H}$ is a Hadamard matrix and $\overline{\boldsymbol{H}}$ the matrix with all the signs reversed, then

$$\begin{array}{cc} \boldsymbol{H} & \boldsymbol{H} \\ \boldsymbol{H} & \overline{\boldsymbol{H}} \end{array} \qquad (4.3)$$

is also a Hadamard matrix. Generally, the entire set of 2^k matrices is constructed by recursive expansion, using Kronecker multiplication:

$$\boldsymbol{H}_{2N} = \boldsymbol{H}_N \otimes \boldsymbol{H}_2 \qquad (4.4)$$

There is also an important subset of Hadamard matrices for $N = 4n$, where n is a positive integer. Hadamard discovered the matrices of this kind for $N = 12$ and 20. It is believed that all such $4n$ matrices exist; this has been proved at least up to $N = 264$. The Appendix sets out some of the Hadamard matrices that are useful for NMR.

4.1.1 Hadamard Encoding

But why would an NMR spectroscopist be interested in such an arcane branch of mathematics?[4] An illuminating example is provided by localized in vivo spectroscopy, in particular the procedure developed by Bolinger and Leigh.[5] Selective excitation in a set of three orthogonal applied magnetic field gradients generates an NMR signal from a single, well-defined voxel, but the sensitivity is naturally low because the spins in most of the sample remain dormant. The measurement must be repeated several times with different sets of irradiation frequencies to map out the spatial dependence of the NMR spectrum. The "multiplex advantage" has been lost, but it can be retrieved by multivoxel localization, in which N voxels are excited simultaneously, with the senses of the radiofrequency excitation pulses encoded according to the rows of the matrix $\boldsymbol{H}_N$ in N consecutive experiments, using a new row as the coding pattern for each scan. All the spins in the sample are active in every scan. The decoding process (essentially a Hadamard transform) is achieved by multiplying the observed signals by the transpose of the original encoding matrix. For example, if $N = 4$ this product is four times the 4×4 identity matrix:

$$\begin{matrix} 4 & 0 & 0 & 0 \\ 0 & 4 & 0 & 0 \\ 0 & 0 & 4 & 0 \\ 0 & 0 & 0 & 4 \end{matrix} \qquad (4.5)$$

In the general case, all the signals from N voxels are separated, and they are N times stronger than would be detected in the pedestrian single-voxel mode, whereas the noise increases only as $\sqrt{N}$. This $\sqrt{N}$ sensitivity improvement is the key to the applications of Hadamard encoding in NMR.

An everyday analogy[6] is often used to make this important point. Weighing a set of N different objects on a balance is usually carried out one object at a time. However, there is always a small random error in the weighing process. Repeating each and every measurement p times would reduce these statistical errors but would involve an unacceptable investment in time, proportional to pN. The trick is to place all N objects on the balance at the same time, and then repeat the weighing N times, each time encoding the information according to the rows of the Hadamard matrix of order N. By convention the standard weights are on the right-hand pan; encoding is achieved by moving an object from the left-hand pan (+) to the right-hand pan (−). At the end of N measurements, the results are decoded according to the columns of the same matrix, giving N times the individual weights. The statistical weighing errors increase as $\sqrt{N}$, so the measurement precision is improved by $\sqrt{N}$.

For this reason, Hadamard spectroscopy benefits from the same multiplex advantage as Fourier spectroscopy; indeed it enjoys a slight advantage, because full amplitude signals (positive or negative) are recorded, as opposed to signals modulated by a cosine wave. In other words, Walsh square-wave functions have replaced the cosine functions. This offers a distinct advantage for digital calculations; the Hadamard transform is much faster than the Fourier transform.

4.2 HADAMARD SPECTROSCOPY

Fourier spectroscopy elicits the impulse response of a spin system. This is sometimes likened to attacking a grand piano with a sledgehammer—all the notes are excited at the same time. If the right sheet music is available, perhaps we should consider playing only a selected set of keys? To apply this idea to high-resolution NMR[7] requires a scheme for multiple irradiation, essentially an array of selective radiofrequency pulses.[8] The individual frequencies are obtained by phase-ramping, and are combined by vector addition in a waveform generator. A demonstration of the potential of this technology is provided in Figure 4.1. This experiment used 2048 separate excitation frequencies, spanning a crowded 2 kHz region of the 500 MHz high-resolution NMR spectrum of strychnine.[9] It employed a *uniform* comb of frequencies at 1 Hz intervals, modulated plus or minus according to the rows of a Hadamard matrix of order 2048. The resulting proton spectrum is essentially indistinguishable from the conventional Fourier transform spectrum, but since it required 2048 scans,

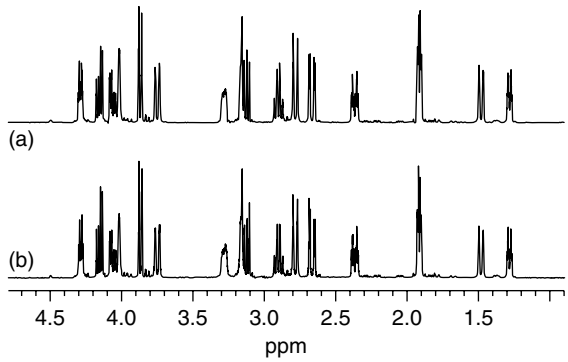

Figure 4.1. (a) One-dimensional Hadamard spectrum of protons in strychnine, recorded at 500 MHz using 2048 separate selective irradiation channels spaced 1 Hz apart, encoded according to a Hadamard matrix of order 2048. This is shown to emphasize the power of multiple selective excitation. (b) The conventional Fourier transform spectrum is virtually indistinguishable. (Reproduced from Ref. 9. © Elsevier, 2003.)

it has little practical use in this form. However, by limiting and tailoring the excitation pattern, it can be adapted for solvent suppression, multiple selective decoupling, or for data-reduction schemes. It is shown here merely to demonstrate how readily multiple-irradiation experiments can be implemented on a modern high-resolution spectrometer.

The Hadamard method comes into its own when applied to multidimensional NMR. Despite the undisputed success of multidimensional methods, particularly for large molecules such as proteins, there is one important practical limitation. It is necessary to examine every increment in every evolution dimension while satisfying the Nyquist sampling condition and the resolution requirements. For example, a three-dimensional experiment with 256 increments in each of the two evolution dimensions and just one second for acquisition and relaxation recovery would have a total duration of over 18 h. While this might be acceptable in some circumstances, higher-dimensional versions with comparable parameters would be quite unrealistic. Sacrifices have to be made. Generally these fall under the heading of sparse sampling—truncation of the evolution periods followed by linear prediction of the "lost" data, controlled aliasing, random sampling, or exponentially weighted sampling (see Chapters 5–10). These schemes inevitably produce artefacts, and they have only a modest impact on the total duration; they are mere palliatives. An interesting exception is limited radial sampling, which generates plane projections after Fourier transformation, and permits reconstruction from the projections (see Chapter 5).

Selective excitation addresses the situations where the information required is quite limited—only a few chemical sites are involved. An *essential* feature is the necessity for prior knowledge of the appropriate chemical shifts. Many structural problems can often be solved by a limited set of selective one-dimensional experiments. The only drawback is the loss of sensitivity compared with a two-dimensional Fourier transform experiment which enjoys the multiplex advantage. By analogy with the multivoxel excitation experiments mentioned above, Hadamard encoding restores the multiplex advantage. When the number (C) of key chemical sites is relatively small, only $N \geq C$ scans are required and the measurement is rapidly completed.

The effectiveness of the Hadamard scheme has been demonstrated in an experiment to explore eight different one-bond ^{13}C–H splittings in the 400 MHz correlation spectrum of an equilibrium mixture of α- and β-D-glucose.[10] Eight scans were used, with the soft radiofrequency excitation pulses encoded according to the Hadamard matrix of order 8. A clean separation of the eight different subspectra was achieved. Similar Hadamard schemes have been extended to the detection of *long-range* ^{13}C–H splittings in strychnine.[11]

Hadamard spectroscopy encodes the NMR information as positive or negative signals. This is actually a special case of a more general scheme for *phase-encoding*,[12] where the N channels have phase increments $2\pi/N$. An $N \times N$ encoding matrix is employed, but in contrast to the Hadamard scheme, N can now take any value. Composite free induction decays are acquired and then separated into N "pure" components. Suppose that the first column of the encoding matrix has all signals with phase zero, then all the remaining columns comprise N signal vectors uniformly distributed around a circle, leaving zero resultants. To extract the signal from the second column, the receiver phase advances in steps of $2\pi/N$; for the third column in steps of $4\pi/N$, etc. This separation process is essentially a Fourier transformation. Note the advantage that N can be exactly matched to C, the number of chemical sites under investigation.

4.2.1 Two-Dimensional Spectroscopy

Structural chemists have long known how to identify chemical sites that are related by spin–spin coupling, spatial proximity or chemical exchange, because there are double-resonance experiments that yield this information. Unfortunately, they can be slow and tedious to perform. The breakthrough came with Jeener's concept of two-dimensional NMR and Ernst's generalization of the method. A simple two-dimensional contour map supplies a clear pictorial representation of the desired "correlations". An important example is the "COSY" spectrum, where spin-spin interactions are represented as off-diagonal "cross-peaks", whereas all the passive NMR responses fall on the principal diagonal $F_1 = F_2$ (see Chapters 12 and 13). This is just the kind of graphic display most suited to the way a structural chemist visualizes the problem.

Now it is possible to perform a "pseudo-COSY" experiment by stacking together the results of a long sequence of double-resonance measurements, stepping the irradiation frequency through the entire proton spectrum in small regular increments. This ψ-COSY spectrum[13] is essentially equivalent to the conventional COSY spectrum, except that the diagonal peaks have rather lower intensity. While this double-resonance mode of operation might seem a retrograde step in comparison with the conventional COSY mode, it does have the advantage that attention can be focused on selected regions with high resolution, whereas the conventional Fourier mode records the full width of the spectrum. The ψ-COSY mode has the advantage of flexibility in the choice of information to be displayed.

Once we accept that prior knowledge of the chemical shifts is necessary and easily obtained, a far more effective Hadamard mode can be implemented to generate two-dimensional spectra. Instead of the conventional COSY scheme employing an evolution interval t_1, followed by two-dimensional Fourier transformation, this new experiment explores the F_1 dimension directly with a set of simultaneous selective radiofrequency pulses, each tuned to one of the chemical shift frequencies. Only one stage of Fourier transformation is employed. If there are C chemical shifts involved, N scans are performed with the excitation pulses encoded according to a Hadamard matrix of order N, where $N \geq C$. The efficiency increases as N approaches C, hence the importance of having a range of low-order Hadamard matrices available, for example, $N = 4$, 8, 12, 16, 20, 24, 28, or 32. The (composite) free induction decays from N successive scans are then decoded according to the appropriate columns of the matrix, and Fourier-transformed. A two-dimensional experiment has been replaced by a limited set of one-dimensional measurements, but all the essential correlation information is retained. The resulting F_2 traces are fed into a contour-plotting routine, taking account of the discontinuities in the F_1 dimension. The concept is not of course restricted to COSY spectra; TOCSY (total correlation spectroscopy), NOESY (nuclear Overhauser effect spectroscopy), HSQC (heteronuclear single-quantum correlation), HMQC (heteronuclear multiple-quantum correlation), HMBC (heteronuclear multiple-bond correlation), or more sophisticated sequences can be tailored to the Hadamard mode, using encoded selective 180° pulses where appropriate. Solid-state Hadamard investigations have also been carried out.[14]

Whereas Fourier transform two-dimensional spectra normally employ phase cycling (an additional time factor of four) and quadrature detection in the F_1 dimension (an additional factor of 2), the Hadamard mode can dispense with these complications. Suppose that the Nyquist condition and the resolution requirements demand a total of E increments in the evolution dimension of the conventional experiment. Neglecting the short time required to determine the chemical shifts from a prior one-dimensional measurement, the speed advantage of the Hadamard mode over the conventional approach would then be $8E/N$, which can be quite a large number. This speed advantage would be particularly large for wide spectral widths such as those experienced in ^{13}C, ^{15}N, ^{19}F, or ^{31}P systems.

4.2.2 Fine Structure of Cross-Peaks

Suppose we wish to record a two-dimensional proton TOCSY spectrum with all its associated fine structure without resorting to a protracted two-dimensional experiment that would require a very large number of increments in the evolution dimension (t_1). At first sight, it might appear that limited frequency-domain excitation has little to offer in this application, in view of the coarse steps in the F_1 dimension. However, the situation is saved by the inherent symmetry of an ideal TOCSY spectrum with respect to the principal diagonal ($F_1 = F_2$). A Hadamard experiment with

sparse sampling in F_1 can in fact retrieve all the fine structure, because the cross-peaks always occur in symmetrically related pairs, and because the F_2 dimension is finely digitized.

Consider the case of the crowded 1.4–3.3 ppm region of the 700 MHz TOCSY spectrum of strychnine. Total correlation spectroscopy relies on homonuclear Hartmann–Hahn transfer of coherence between sites that have experienced a differential perturbation of the spin populations. Suppose we restrict the selective irradiation to just 15 radiofrequencies, each covering a 45 Hz band. These are "tuned" to the chemical shifts obtained from a prior low-resolution one-dimensional experiment. Gaussian 180° spin-inversion pulses are applied at the sites designated by "+" in the rows of the Hadamard H_{16} matrix, while sites designated by "−" are left unperturbed. (The "all +" row is not used as it is ineffective for Hartmann–Hahn transfer.) After an isotropic mixing period, a hard 90° pulse elicits a composite signal consisting of all the free induction decays. These are then separated into 15 individual free induction decays by Hadamard decoding, and Fourier-transformed.

Cross-peaks in conventional TOCSY spectra occur in pairs, and if the instrumental broadening is the same in both dimensions, their fine structures

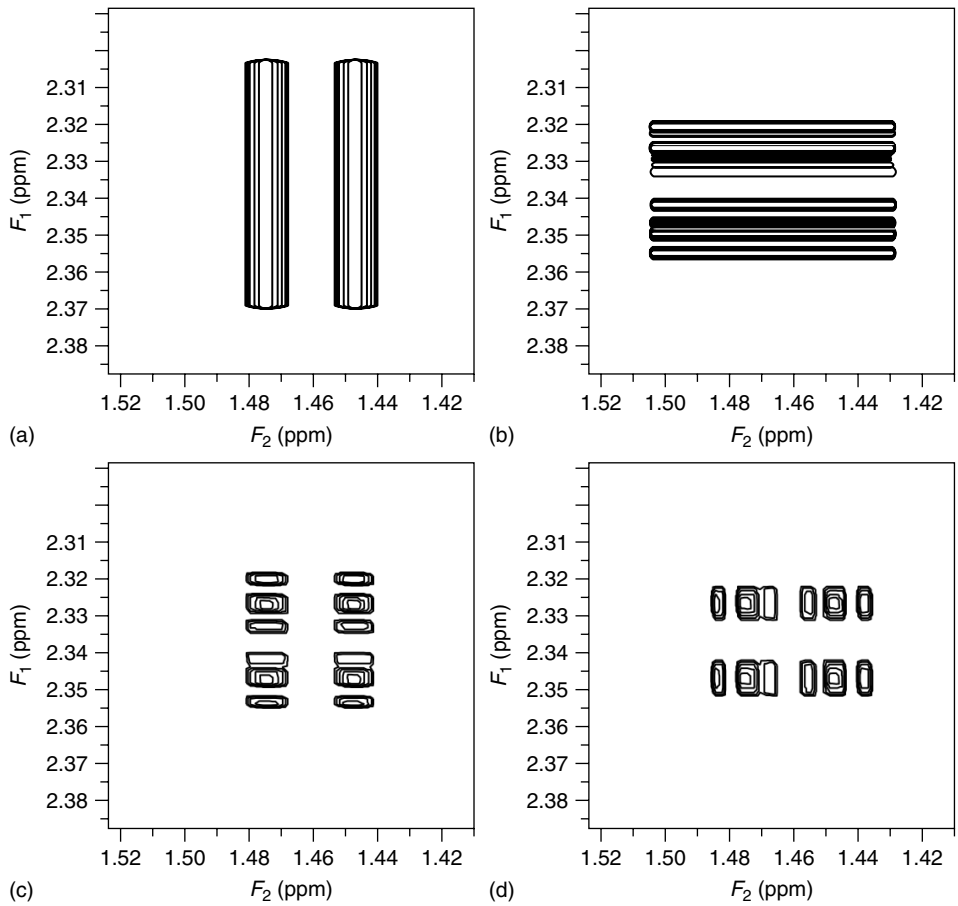

Figure 4.2. Procedure for reconstructing a pair of cross-peaks in a TOCSY spectrum starting with F_2 traces at the relevant chemical shifts. (a) The first F_2 trace convoluted in the F_1 dimension with a 45-Hz rectangular function. (b) The second F_2 trace convoluted in the same manner and then rotated through 90°. (c) The superposition of (a) and (b) processed (pixel by pixel) by the lower-value algorithm. The elongated features are suppressed. (d) The other cross-peak, obtained by rotating (c) through 90°. (Reproduced from Ref. 16. © Elsevier, 2003.)

are exactly related as mirror images reflected about the principal diagonal. That is to say, the S → I cross-peak and its "twin" I → S cross-peak are related by a 90° rotation.[15] Although this "ideal world" symmetry is broken in the Hadamard mode, all the desired fine structure can be derived from the high-resolution F_2 traces passing through each cross-peak of the pair. These two F_2 traces contain all the information needed to reconstruct an entire cross-peak with well-resolved multiplet structure in both dimensions.

The processing involves convolution of each F_2 trace with a 45 Hz wide rectangular function in the F_1 dimension. If we imagine this in terms of intensity contours, these are elongated in F_1 but well resolved in F_2 (Figure 4.2a). The second cross-peak is rotated through 90° (Figure 4.2b) so that the elongation of these contours is at right angles to the elongation in Figure 4.2(a). The two patterns are now superimposed. Fine digitization is restored in both dimensions by comparing intensities in the superposition, pixel by pixel, retaining the lower value (all the signals are positive). In this way, the elongated regions are suppressed; only the narrow features survive (Figure 4.2c). The reconstructed twin cross-peak is obtained by a 90° rotation (Figure 4.2d). The resulting (symmetrized) Hadamard spectrum of strychnine (Figure 4.3) shows the desired fine structure in both frequency dimensions, with one cross-peak highlighted on an expanded frequency scale.[16]

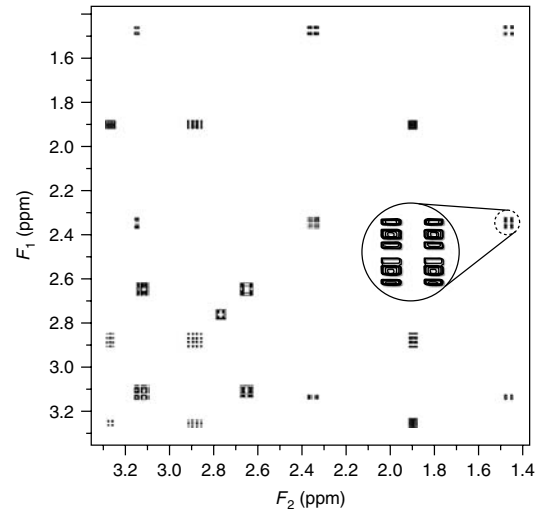

Figure 4.3. High-resolution 700 MHz TOCSY spectrum of strychnine in the crowded region between 1.4 and 3.3 ppm, excited by frequency-domain spin-inversion pulses encoded by the $\boldsymbol{H}_{16}$ matrix. Only 15 chemical sites were irradiated and the measurement was complete in 42 s. Although the F_1 increments were necessarily coarse, the fine structure of the cross-peaks is revealed by a symmetrization procedure (*see* Figure 4.2), and illustrated on an expanded frequency scale for one selected cross-peak (inset). (Reproduced from Ref. 16. © Elsevier, 2003.)

4.2.3 A Two-Dimensional Hadamard Spectrum

The utility of frequency-domain excitation is best illustrated by a concrete example, the Hadamard TOCSY spectrum of erythromycin A, recorded at 800 MHz.[17] Using chemical shifts from a prior one-dimensional proton spectrum, 22 sites were selected for excitation, with the soft radiofrequency pulses encoded on or off according to 22 rows of the $\boldsymbol{H}_{28}$ matrix avoiding the "all +" row. A total of 28 scans was required. Decoding employed the 22 corresponding columns of the matrix, generating a separate free induction decay for each site. Fourier transformation of these free induction decays gave a set of 22 traces running in the F_2 dimension. These traces contain all the desired correlation information, but for presentational purposes, it can be useful to reconstruct a two-dimensional contour map, which required the symmetrization routine described above. The experimental duration, including twofold time-averaging and two initial dummy runs to establish steady-state conditions, was 2 min 33 s. The result (Figure 4.4) is essentially equivalent to the conventional spectrum obtained in the Fourier transform mode which required 256 evolution increments. However there is a 68-fold reduction in the time required to complete the measurement. In the Hadamard mode the diagonal peaks are markedly less prominent, which can be an advantage for detecting cross-peaks close to the diagonal.

4.2.4 Protein Spectra

Protein chemists often apply multidimensional NMR methods to samples globally enriched in ^{13}C and ^{15}N, with a view to simplifying the spectra. The conventional procedure is to allow the ^{13}C or ^{15}N resonances to evolve freely before transferring coherence back to protons. In contrast, the Hadamard

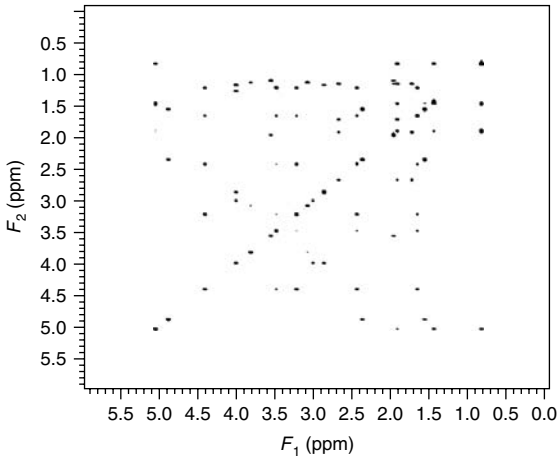

Figure 4.4. A selected region of the 800 MHz proton TOCSY spectrum of erythromycin A recorded in 2 min 33 s by the Hadamard technique. The 22 chosen sites were irradiated with spin-inversion pulses encoded according to the $\boldsymbol{H}_{28}$ matrix. The contour map was reconstructed using a symmetrization routine acting on the well-resolved F_2 traces (see text). (Reproduced by permission of © Elsevier, 2003.)

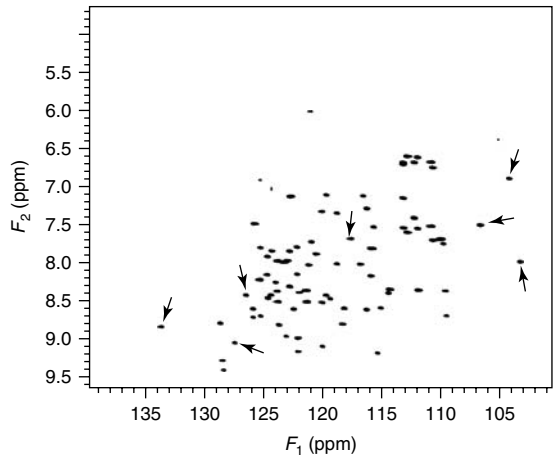

Figure 4.5. The 800 MHz two-dimensional HSQC spectrum of human ubiquitin recorded by the conventional method, showing the $^1H-^{15}N$ correlations. With a four-step phase cycle and quadrature detection in the F_1 dimension the experimental duration was 23 min 51 s. The seven ^{15}N sites indicated by arrows were selected for the Hadamard experiments. (Reproduced by permission of © Elsevier, 2003.)

mode dispenses with evolution periods altogether, but applies selective radiofrequency spin-inversion pulses at the ^{13}C or ^{15}N frequencies, modulated on or off. This imposes an important limitation on the Hadamard scheme, because prior information about the relevant ^{13}C or ^{15}N chemical shifts can be difficult to measure, even in isotopically enriched samples. Therefore, Hadamard spectroscopy is not considered as the first line of attack on an unknown protein; it serves rather as a supplementary technique to extract further information once the conventional spectrum has been acquired.

Below are some examples of this approach applied to a well-studied protein, ubiquitin (0.3 mM) investigated on an 800 MHz spectrometer.[17] Once the two-dimensional $^1H-^{15}N$ correlation spectrum has been recorded by conventional HSQC spectroscopy (Figure 4.5), seven amide sites can be chosen for selective irradiation with Gaussian 180° pulses, coded on or off according to the $\boldsymbol{H}_8$ matrix. The measurement duration is reduced from 23 min 51 s in the conventional mode to just 13 s, two orders of magnitude faster. Selective excitation has the effect of converting the *global* isotopic labeling into the equivalent of *specific* labeling, something that is quite expensive to achieve by standard chemical methods. Often it is the environment of the active site of the protein that matters; the rest of the spectrum is essentially irrelevant. The result is a vastly simplified subspectrum (Figure 4.6), which serves as the starting point for more specific investigations.

4.2.4.1 Chemical Exchange

Bougault *et al.*[18] have adapted Hadamard method to extract information about the exchange rates of ubiquitin amide protons with deuterons in the solvent. The exchange rates cover a vast range, with a strong dependence on pH, but the conventional techniques can measure only very fast or very slow exchange. It is the appreciable duration of a two-dimensional NMR spectrum that inhibits the investigation of the intermediate rates. The solution is to use Hadamard spectroscopy at the seven chosen amide sites, thus decreasing the duration of the experiment by a factor of about 32. The sample was 90% labeled with ^{15}N at the amide sites and the measurements were performed at the physiologically relevant pH of 6.2. These seven amide sites showed a wide range of decay rates (Figure 4.7) providing evidence that some residues were more exposed to the solvent (^2H_2O) or closer to ionizing groups than others.

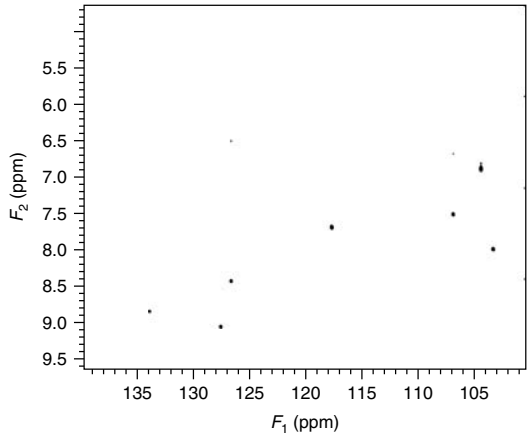

Figure 4.6. The Hadamard subspectrum corresponding to the seven selected sites indicated in Figure 4.5. Gaussian 180° pulses with an effective bandwidth of 20 Hz were used for spin inversion, coded on or off according to $\boldsymbol{H}_8$. Total measurement duration was 13 s. (Reproduced by permission of © Elsevier, 2003.)

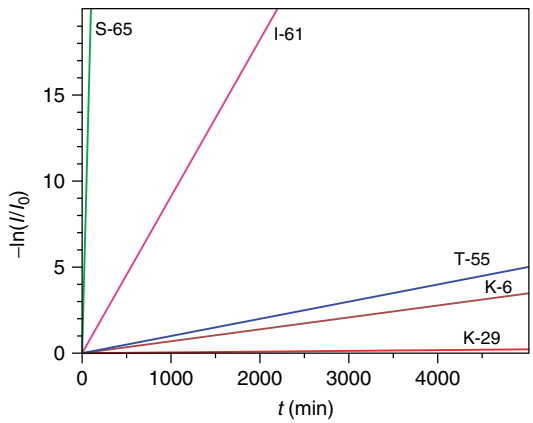

Figure 4.7. Decay rates $-\ln(I/I_0)$ of proton signals from seven chosen amide groups in ubiquitin exchanging with deuterium from the solvent. The encoding used the $\boldsymbol{H}_8$ matrix to control the selective 180° spin-inversion pulses applied to ^{15}N. (Reproduced from Ref. 18. © Springer, 2004.)

4.2.4.2 Accurate NH Splittings

Important structural information can be elicited by measuring residual dipolar couplings in a medium that partially aligns the solute molecules, increasing or decreasing the observed splittings, depending on

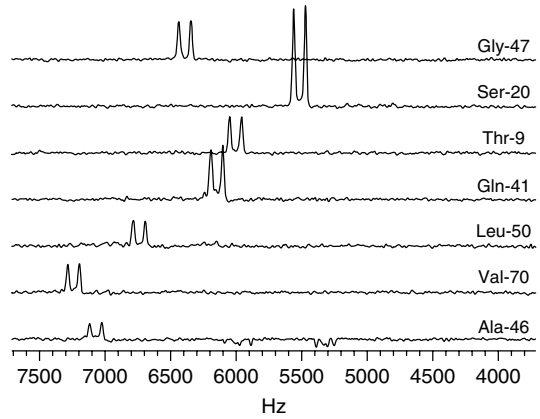

Figure 4.8. Traces from the 800 MHz Hadamard spectrum of ubiquitin showing the ^{15}N–H splittings in the seven selected residues with high definition. Although this was in fact an isotropic solution, the results suggest that the method could be used to derive precise values for residual dipolar couplings in a partially oriented medium. (Reproduced by permission of © Elsevier, 2003.)

the orientation of the appropriate internuclear vectors (see Chapters 1, 29 and 30). When the requisite prior knowledge of chemical shifts has been obtained, selective Hadamard experiments can focus attention on specific chemical sites with good sensitivity and fine digital resolution, thus permitting precise measurement of the desired splittings. Figure 4.8 illustrates the *feasibility* of the Hadamard mode for the determination of N–H splittings,[17] although in this case, the seven selected traces are from an *isotropic* solution of ubiquitin. Even with fine resolution (0.5 Hz) and time-averaging of eight transients to improve sensitivity, this measurement required only 90 s by the Hadamard protocol.

4.2.4.3 Dynamic Measurements

Protein spectra are normally too crowded to permit investigation of the dynamic properties of individual sites, but the simplification offered by Hadamard spectroscopy facilitates the study of such time-dependent phenomena. The seven selected amide sites of ubiquitin provide a practical example. Spin-lattice relaxation curves for ^{15}N were recorded by repeating the fast Hadamard experiment for a range of different recovery times at 0.1 s intervals. Figure 4.9 illustrates the results from one such case

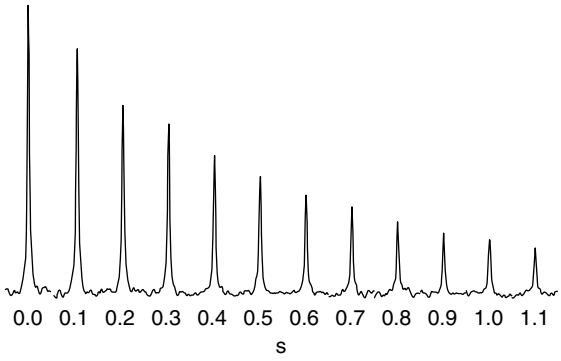

Figure 4.9. Spin-lattice relaxation curves for ^{15}N were measured at the seven chosen amide sites of ubiquitin using the Hadamard scheme. The relaxation of the Gly-47 residue is shown for illustration, indicating $T_1 = 0.57 \pm 0.01$ s. (Reproduced by permission of © Elsevier, 2003.)

(the residue Gly-47) with a T_1 value of 0.57 ± 0.01 s at 25°C.[17]

4.3 HIGHER DIMENSIONS

The problem of long experimental durations is exacerbated in multidimensional spectroscopy. Although the requisite large number of scans increases the signal-to-noise ratio, many modern NMR spectrometers, particularly those equipped with a cryogenically cooled probe, achieve an adequate level of sensitivity long before all the evolution dimensions have been completely explored. Noise is no longer the major criterion; speed is the critical parameter. Some protein studies tie up an expensive spectrometer for days at a time.

It is quite feasible to nest two or more stages of Hadamard encoding one within another, paving the way for experiments in which each evolution stage is replaced by irradiation with a different set of selective radiofrequency pulses. If the cascaded Hadamard matrices have orders $N, P, Q, \ldots$ the overall measurement duration increases as the product $NPQ\ldots$, but the individual speed advantages are also multiplicative, giving extremely large speed factors indeed.

Consider the three-dimensional case. Two sets of selective ^{13}C and ^{15}N spin-inversion pulses invert the sign of the final proton response in a pattern determined by the interplay between the two cascaded Hadamard matrices. After two stages of decoding, the resulting free induction decays are converted into F_3 traces by Fourier transformation. These traces contain all the requisite C–H, C–N, or N–H correlation information, but for a more pictorial representation,

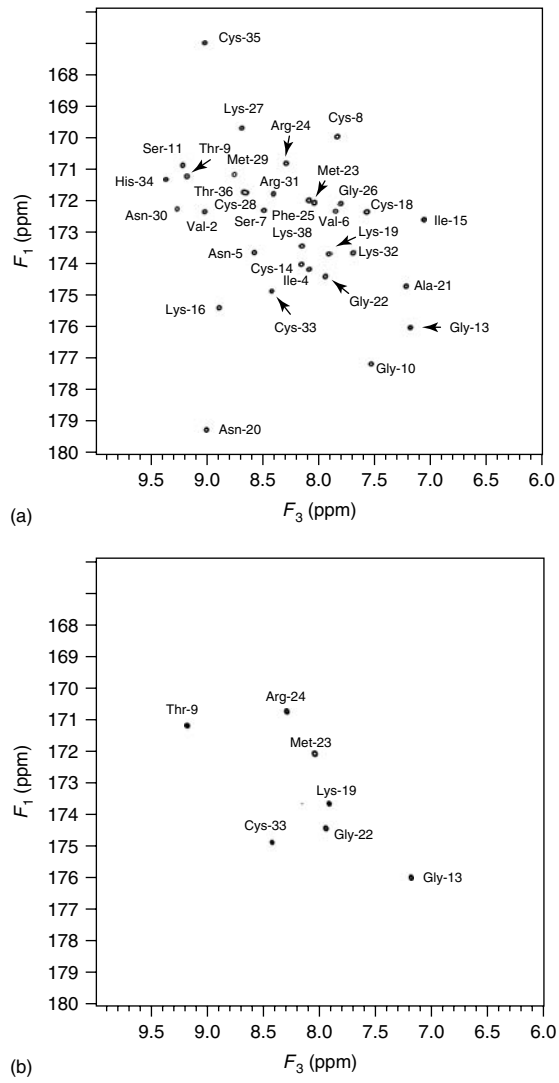

Figure 4.10. (a) The conventional three-dimensional HNCO spectrum of agitoxin projected onto the F_1F_3 plane, showing the ^{1}H–^{13}C correlations. Seven sites were chosen arbitrarily, indicated by the arrows. (b) The Hadamard subspectrum of these seven sites, showing a speed advantage of more than 200. (Reproduced by permission of © Elsevier, 2003.)

they can be converted into a three-dimensional data matrix and projected onto any one of the three orthogonal planes F_1F_3, F_1F_2, or F_2F_3.

An illustrative example is provided by the three-dimensional HNCO spectrum of a 4 kDa protein, agitoxin, studied as a 0.3 mM aqueous solution on a 700 MHz spectrometer.[19] A conventional three-dimensional experiment, of duration 20 h 43 min, generates a three-dimensional matrix that can be projected onto the $^1H-^{13}C$ plane or the $^1H-^{15}N$ plane (Figure 4.10a). With this prior knowledge of the ^{13}C and ^{15}N chemical shifts, a three-dimensional Hadamard experiment was set up. Seven arbitrary sites were chosen, indicated by the arrows in Figure 4.10(a). The effective bandwidth of the soft radiofrequency inversion pulses was 45 Hz for both ^{13}C and ^{15}N. Encoding (on/off) followed the pattern decreed by two nested $\boldsymbol{H}_8$ matrices, avoiding the "all plus" rows which tend to be more sensitive to instrumental shortcomings. This entailed a total of 64 scans. Broadband decoupling was used to collapse the C–H, N–H, and C–N splittings. Figure 4.10(b) shows the three-dimensional Hadamard spectrum for the seven chosen residues, which considerably reduces the experimental duration, by a factor of more than 200.

4.4 DISCUSSION

Multidimensional Hadamard spectroscopy offers a useful alternative to the more usual Fourier transform technique. Based on prior knowledge of the chemical shifts from an earlier measurement, an arbitrary set of C frequencies is chosen. These C sites are excited with an array of selective radiofrequency pulses. By encoding the pulses according to a Hadamard matrix of order N, where $N \geq C$, and acquiring N scans, the individual responses are separated by a decoding procedure based on the same Hadamard matrix. Applied to multidimensional experiments, the Hadamard approach saves considerable time as there is no need for systematic step-by-step exploration of all the evolution dimensions. The intrinsic sensitivity enjoys the same multiplex advantage as the corresponding Fourier transform experiment. Multidimensional experiments employ a cascade of nested Hadamard matrices and offer important time savings. However if they involve nuclei such as ^{13}C or ^{15}N, the need for prior knowledge of the ^{13}C or ^{15}N chemical shifts restricts the Hadamard method to a supplementary role, such as the study of time-dependent phenomena or fine details of the spectrum.

4.5 APPENDIX

Some useful low-order Hadamard matrices (reproduced with permission from N. J. A. Sloane, AT&T Shannon Laboratory, 180 Park Avenue, Florham Park, New Jersey, USA). The matrix $\boldsymbol{H}_{16}$ can be derived from $\boldsymbol{H}_8$ using equation (4.1):

$\boldsymbol{H}_8$

```
+ + + + + + + +
+ − + − + − + −
+ + − − + + − −
+ − − + + − − +
+ + + + − − − −
+ − + − − + − +
+ + − − − − + +
+ − − + − + + −
```

$\boldsymbol{H}_{12}$

```
+ − − − − − − − − − − −
+ + − + − − − + + + − +
+ + + − + − − − + + + −
+ − + + − + − − − + + +
+ + − + + − + − − − + +
+ + + − + + − + − − − +
+ + + + − + + − + − − −
+ − + + + − + + − + − −
+ − − + + + − + + − + −
+ − − − + + + − + + − +
+ + − − − + + + − + + −
+ − + − − − + + + − + +
```

$\boldsymbol{H}_{20}$

```
+ + + + + + + + + + + + + + + + + + + +
+ + + + + + + + + + − − − − − − − − − −
+ + + + + − − − − − + + + + − − − − − −
+ + + + − + − − − − + − − − − + + + + − −
+ + + − − − + − − − + + − − + + − − + + −
+ + − + − − + − − − − − + + − − + + − + +
+ + − − + + − − + − − + − + − + − + − + −
+ + − − + − − + − − − + − − + − + − + + −
+ + − − − − + + + + − − + + − − + + − − −
+ + − − − − − + + + + − + + − + − − + − −
+ − + + − − − + + − + − − + + − − + + − +
+ − + − + − + − + − + − + − − − − + + + +
+ − + − + − − + − + − + − + − − + + + − −
+ − + − − + + − − + − − + + + + − + − − −
+ − + − − + − + + − + − − + + − + − − + +
+ − − + + − + − − + + − − + − + + + − − −
+ − − + − + + − + − − + + + − − + − + − −
+ − − + + − − + + − − + − + + + − − + − +
+ − − − + + + + − − + + − − + + − − − + −
+ − − − + + + − − + + − − + + − − + − + −
```

RELATED ARTICLES IN THE ENCYCLOPEDIA OF MAGNETIC RESONANCE

Liquid Crystalline Samples: Application to Macromolecular Structure Determination

Whole Body MRI: Strategies for Improving Imaging Efficiency

REFERENCES

1. M. Ottinger, F. Delaglio, and A. Bax, *J. Magn. Reson.*, 1998, **131**, 373–378.
2. M. Ikura, L. E. Kay, and A. Bax, *J. Magn. Reson.*, 1990, **86**, 204–209.
3. J. Hadamard, *Bull. Sci. Math.*, 1893, **17**, 240–248.
4. (a) R. Kaiser, *J. Magn. Reson.*, 1974, **15**, 44–63; (b) B. Blümich and D. Ziessow, *J. Magn. Reson.* 1982, **46**, 385.
5. L. Bolinger and J. S. Leigh, *J. Magn. Reson.*, 1988, **80**, 162–167.
6. N. J. A. Sloane, in '*Fourier, Hadamard, and Hilbert Transforms in Chemistry*', eds A. G. Marshall, Plenum Press: New York, 1982.
7. (a) J. Ashida, T. Nakai, and T. Terao, *Chem. Phys. Lett.*, 1990, **168**, 523–528; (b) H. R. Bircher, C. Müller, and P. Bigler, *J. Magn. Reson.* 1990, **89**, 146; (c) M. Greferath, B. Blümich, W. M. Griffith, and G. L. Hoatson, *J. Magn. Reson. Ser A* 1993, **102**, 73–80; (d) T. Nishida, G. Widmalm, and P. Sandor, *Magn. Reson. Chem.*, 1995, **33**, 596–599; (e) J. Schraml, H. van Halbeek, A. De Bruyn, R. Contreras, M. Maras, and P. Herdewijn, *Magn. Reson. Chem.*, 1997, **35**, 883–888.
8. Ē. Kupče and R. Freeman, *J. Magn. Reson., Ser. A*, 1993, **102**, 122–126.
9. Ē. Kupče and R. Freeman, *J. Magn, Reson.*, 2003, **162**, 158–165.
10. V. Blechta and R. Freeman, *Chem. Phys. Lett.*, 1993, **215**, 341.
11. V. Blechta, F. del Rio-Portilla, and R. Freeman, *Magn. Reson. Chem.*, 1994, **32**, 134–137.
12. Ē. Kupče and R. Freeman, *J. Magn. Reson. Ser A*, 1993, **105**, 310–315.
13. S. Davies, J. Friedrich, and R. Freeman, *J. Magn. Reson.*, 1987, **75**, 540–545.
14. J. Ashida, Ē. Kupče, and J.-P. Amoureux, *J. Magn. Reson.*, 2005, **177**, 474–480.
15. L. McIntyre and R. Freeman, *J. Magn. Reson.*, 1989, **83**, 635–649.
16. Ē. Kupče and R. Freeman, *J. Magn. Reson.*, 2003, **162**, 300–310.
17. Ē. Kupče, T. Nishida, and R. Freeman, *Prog. NMR Spectrosc.*, 2003, **42**, 95–122.
18. C. Bougault, L. Feng, J. Glushka, Ē. Kupče, and J. H. Prestegard, *J. Biomol. NMR*, 2004, **28**, 385–390.
19. (a) Ē. Kupče and R. Freeman, *J. Biomol. NMR*, 2003, **25**, 349–354; (b) R. Freeman and Ē. Kupče, *J. Biomol. NMR*, 2003, **27**, 101–113.